2021 IEEE International Conference on Robotics and Automation (ICRA 2021)
May 31 - June 4, 2021, Xi'an, China

States and Contact Forces Estimation for a Fabric-Reinforced Inflatable Soft Robot*

Phuc D.H. Bui[1] and Joshua A. Schultz[1]

Abstract— **Soft robots can operate effectively inside confined spaces because their soft bodies can adapt to accommodate the geometry around them. When they interact with the environment, the presence of contact forces can dramatically change the dynamics of the robots. If a soft robot is in contact and the contact force is not known, the control action is still targeted for a free robot. Hence the robot may perform improper actions. Because a soft robot is deformable, it is quite challenging to determine the contact forces and the system states from sensor measurements. This paper proposes an observer design to estimate the states of a fabric-reinforced inflatable soft robot as well as the external contact forces. The soft robot is represented by the disc-thread model which results in a set of ordinary differential equations (ODEs). A linear parameter-varying (LPV) system including some subsystems is formed to represent the nonlinear robot. The observer is based on the sliding mode approach and includes a set of sub-observers corresponding to the subsystems in the LPV system. The observer is validated through simulations and an experiment. The simulation results show that the observer can estimate the angular positions and their rate of changes as well as assumed contact forces with no error in steady states. The experiment results display good tracking of the robot's configurations compared to the ground truth data from the motion tracking system.**

I. INTRODUCTION

Soft robots can adaptively interact with their environment thanks to their deformable bodies. Soft bodies make them suitable for new applications where rigid robots are inapplicable. However, it is more challenging to model soft robots as well as to design controllers or observers for them [1], [2]. Due to the nonlinearity and complexity of the soft robot models, applying well-developed traditional control algorithms to inflatable soft robotics is difficult. There have been some new-developed control schemes for soft robots but they have to partially rely on estimates of the robot configuration [3], [4]. Designed predominantly to have contact with the surrounding environment, soft robots can be better controlled with higher precision if the contact forces are well known. Despite recent advances in soft sensor technologies, complete and simultaneous sensing of soft robot states and contact forces remains a big challenge due to the deformable nature of soft robots [4].

*This work is supported by the NSF grant No. 1935312 EFRI C3 SoRo: Between a Soft Robot and a Hard Place: Estimation and Control Algorithms that Exploit Soft Robots' Unique Abilities

[1]The authors are with Department of Mechanical Engineering, The University of Tulsa, 800 S. Tucker Drive, Tulsa, OK 74104, USA. phuc-bui@utulsa.edu, joshua-schultz@utulsa.edu

We thank John G. Williamson for his support in collecting the data from the experiments

In this paper, we introduce an observer design to estimate both soft robot states and contact forces. The state estimations use position data from markers placed at several locations on the robot body. The estimated contact forces are able to track the assumed contact forces in a simulated scenario. There have been several works about observers for soft robots. Della Santina et al. designed an observer that combines with machine learning to detect contact on the soft robot body [4]. Zhang et al. used finite elements to estimate the configuration matrices [5]. Gillespie et al. used a Kalman filter to integrate accelerations and angular velocities for robot postures [6]. Ataka et al. used multi-stage Extended Kalman Filter to estimate soft robot poses [7]. Rone and Ben-Tzvi estimated the robot states using the displacement of passive cables [8]. Srivatsan et al. used Lie algebra to estimate the shape of a medical snake robot [9]. However, none of these studies perform both state estimation and contact force estimation using a model-based algorithm. In our study, we propose an observer that provides the means to design full-state feedback controllers in free space and under contact. The observer is based on the sliding mode approach applied to a recently developed disc-thread model of a fabric-reinforced inflatable soft robot. In this modeling approach, the soft robot is discretized into N discs connected by $N-1$ threads to represent joins and links, and the equations of motion are formed using Langrangian method. Since the modeling process produces ODEs in the manner of a traditional robot, the observer is model-based and has a closed form for the same class of robot models.

Our specific contributions include the following:

- Developing an LPV system based on disc-thread model to represent the fabric-reinforced inflatable soft robot,
- Designing an observer to estimate the soft robot states and generalized contact forces,
- Setting up a foundation for future model-based closed-loop control of the fabric-reinforced inflatable soft robots.

This article is structured as follows. In Section II, we review the disc-thread model approach and the formulation of the equations of motion. The LPV system and observer design are addressed in Section III. Section IV shows the simulation and experimental results of the observer. The conclusion is presented in Section V.

II. THE DISC-THREAD MODEL

A. Soft Robot Configuration And Frame Assignment

Our soft robot is an inflatable elastomeric chamber made of Smooth-On Dragon Skin 30 silicone that has a thin band

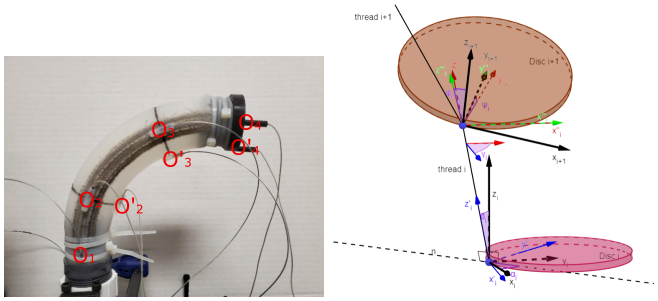

(a) The soft robot with the embedded fabric in the front side and the set of position markers

(b) Disc-thread model

Fig. 1. Examples of configurations of the disc-thread model representing the shape of a soft robot

of fabric embedded longitudinally to reinforce one side. The undeformed shape of the robot body and the fabric band is a circular arc. When inflated pneumatically, the unreinforced side can undergo large strains while the fabric side maintains a constant length. This causes the chamber to bend. Because of the fabric's placement on the robot (see Fig.1a), its tip traces a 3D rather than just a 2D curve.

In order to construct a model that fits naturally with the fabric-reinforced soft robot embodiment, we review the disc-thread model. It was first introduced in [10]. In this approach, we discretize the chamber longitudinally into a sequence of N discs, each connected to its neighbors on either side by a single inextensible thread (representing the fabric reinforcement). Each disc is considered to be a rigid body and is constrained only by the thread. The frame assignments and their implications are illustrated in Fig. 1b.

Each pose of the soft robot is configured by the relative position and orientation between two adjacent discs. Consider a robot with N discs; there will be $N-1$ threads connecting them. As each thread imposes a holonomic constraint, if one end of the robot is fixed, the number of degrees of freedom for the robot is $5(N-1)$. In other words, the coordinate of each disc is parameterized by 5 generalized coordinates. Each disc will be given the subscript i, with $i=1$ corresponding to the root disc. The z axis for frame i will be directed along the normal to the disc, the y axis pointing toward the centroid of the disc and the x axis will be tangent to the circular profile of the disc. Proceeding to the next disc, there will be a corresponding frame with subscripts $i+1$. The generalized coordinates will be defined with regard to three intermediate frames between frame i and $i+1$, each successive one denoted with an additional prime. The thread i is parameterized by two angles $\alpha_i, \beta_i \in [0;\pi]$. Specifically, the other end of the thread i at the disc $i+1$ can move abound an unique axis n which is in (x_i, y_i) plane. α_i is the angle between this n axis and x_i axis and β_i is the angle between the thread i and z_i axis. Performing the rotation (α_i,β_i) on (x_i, y_i, z_i) frame will result in the frame (x_i', y_i', z_i'). The subsequent frames will involve a translation along the inextensible thread (of a fixed distance ℓ_i), together with three other rotations γ_i, ψ_i and ϕ_i, where the twisting of the robot is accounted by γ_i. By performing each of the sequence of rotations to the frame of disc i, it will be aligned with the frame of disc $i+1$. Therefore, the homogeneous transformation matrix from frame i to frame $i+1$ is:

$$ {}^{i}_{i+1}T = T(\alpha_i, \beta_i)T(\gamma_i)T(\psi_i)T(\phi_i), \tag{1} $$

The transformation consisting of 5 variable rotations and a fixed translation accounted for in $T(\gamma_i)$. So by relying on these fictitious discs and threads as well as angles from α_1 to $\phi_{5(N-1)}$, this approach models the soft robot in the manner of a rigid one, but with a higher number of variables.

B. Equation of Motion

With the kinematics of the soft robot fully defined by the disc-thread model, we can then form the Lagrangian and take its derivatives to find the equations of motion using the Euler-Lagrange formulation. The elasticity of the air can be modeled by treating the air as an ideal gas, which exerts a normal force on the N^{th} disc in the z_N direction. The elasticity of the walls can be modeled by connecting springs from some origin on disk i to insertion on disk $i+1$. Since this is a purely rotational system with no prismatic joints, the equations for relating terms such as kinetic energy, potential energy can be formulated primarily based on the relative angular velocity between two adjacent discs. The equation of motion has the form:

$$ \frac{d}{dt}\left(\frac{\partial \mathcal{L}}{\partial \dot{\mathbf{q}}}\right) - \frac{\partial \mathcal{L}}{\partial \mathbf{q}} + \mathbf{A}_{\mathbf{q}}^{T}\boldsymbol{\lambda} = \mathbf{Q} \tag{2} $$

where $\mathbf{q} \in \mathbb{R}^{5(N-1)}$ is the configuration vector containing $\alpha_1 \cdots \phi_{N-1}$ variables, $\frac{\partial \mathcal{L}}{\partial \mathbf{q}}$ is the partial derivative of the Lagrangian with respect to each generalized variable, $\mathbf{Q} \in \mathbb{R}^{5(N-1)}$ is the generalized forces due to the internal pressure acting on the surface of the last disc, and $\mathbf{A}_{\mathbf{q}} \in \mathbb{R}^{5(N-1)\times 5(N-1)}$ is the Jacobian of the Pfaffian constraints arranged so that it can be multiplied by the vector of Lagrange multipliers $\boldsymbol{\lambda} \in \mathbb{R}^{5(N-1)}$. In this study, we examine the soft robot in free and in-contact condition, so we can replace $\mathbf{A}_{\mathbf{q}}^{T}\boldsymbol{\lambda}$ by $\mathbf{F}_c \in R^{5(N-1)}$ which stands for the affects of a contact force on the robot configuration. By using the canonical momenta vector $\mathbf{p} = \frac{\partial \mathcal{L}}{\partial \dot{\mathbf{q}}} = \mathbf{M}\dot{\mathbf{q}}$ with $\mathbf{M} \in \mathbb{R}^{5(N-1)\times 5(N-1)}$ is the mass matrix, we can rewrite the above equation of motion in the state space form as:

$$ \begin{pmatrix} \dot{\mathbf{q}} \\ \dot{\mathbf{p}} \end{pmatrix} = \begin{pmatrix} 0 & \mathbf{M}^{-1} \\ 0 & 0 \end{pmatrix} \begin{pmatrix} \mathbf{q} \\ \mathbf{p} \end{pmatrix} + \begin{pmatrix} 0 \\ \frac{\partial \mathcal{L}}{\partial \mathbf{q}} + \mathbf{Q} - \mathbf{F}_c \end{pmatrix} \tag{3} $$

Note that our soft robot used to characterize the workspace properties of this architecture, described in [11]. The disc-thread model approach and the soft robot equation of motion were presented in [10] and the details will follow in a forthcoming publication.

III. Observer Design For The Soft Robot

Due to the deformable-body of the soft robot, the numerical values of $\mathbf{q}$, $\mathbf{p}$ and $\mathbf{F}_c$ in (3) can not be obtained directly from measuring equipment. In this section, we build an observer to estimate those components using data from a set of position markers and an assumed contact.

The inflatable soft robot described in section II will operate at different pressures (see Fig. 2). At each pressure (operating point), the robot has a different pose due to the changing pressure and the elements of $\mathbf{M}$, $\partial\mathcal{L}/\partial\mathbf{q}$ and $\mathbf{Q}$ in (3) are also changing in a manner corresponding to the current pose of the robot. Note that the values of these matrices must be numerically calculated because they include partial derivatives of expressions of many variables. Therefore, in order to simulate and analyze the system at a certain operating point, numerical values of $\mathbf{M}$, $\partial\mathcal{L}/\partial\mathbf{q}$ and $\mathbf{Q}$ are fed into the equation of motion (3) from separate subroutines. In that case, we can retrieve an affine linear-time-invariant state space standing for the soft robot nearby that operating point. In order to describe the robot throughout its entire range of motion, we divide the entire system into K subsystems fixed to a sequence of operating points, by evaluating the constituent matrices at corresponding pressures and form a switched LPV system. Note that input pressure is chosen as the switching condition because it is the main source that changes the robot configuration. It is also easy to be measured and we don't have to know the robot pose explicitly to choose the correct operating points. The LPV system consists of a set of linear systems whose state-space operational modes are driven by an underlying decision process based on that time-varying pressure. The LPV system is expressed as:

$$\begin{aligned}\dot{\mathbf{x}}(t) &= A_{v(P)}\mathbf{x}(t) + B_{v(P)}u(t) + \Theta_{v(P)} \\ \mathbf{y}(t) &= C\mathbf{x}(t)\end{aligned} \tag{4}$$

where $\mathbf{x} = [\mathbf{q}\ \mathbf{p}]^T = [\mathbf{x}_1\ \mathbf{x}_2]^T$, the output $\mathbf{y} \in \mathbb{R}^m$ is position measurements from motion capture markers (7 in our example). The output is related to the states by $C = [C_1^{m\times m}\ 0] \in \mathbb{R}^{m\times n}$ which results from the linearization of the nonlinear functions mapping the measured data to the world frame. The switching rule $v(P) \in S^K \doteq \{1, 2, ...K\}$ depends on input pressure P. For each $j \in S^K$, the subsystem matrices A_j, B_j and Θ_j take on constant values and have the forms:

$$\begin{aligned} A_j &= \begin{bmatrix} 0 & \mathbf{M}_j^{-1} \\ 0 & 0 \end{bmatrix} \\ B_j &= \begin{bmatrix} 0 \\ \mathbf{Q}_j \end{bmatrix} \\ \Theta_j &= \begin{bmatrix} 0 \\ \left(\dfrac{\partial\mathcal{L}}{\partial\mathbf{q}}\right)_j + \mathbf{Q}_j - \mathbf{F}_{cj} \end{bmatrix} \end{aligned} \tag{5}$$

The number of operating points and their distribution are carefully selected so that the switched LPV system can adequately represent the whole continuous system. The system is considered under the following Assumption.

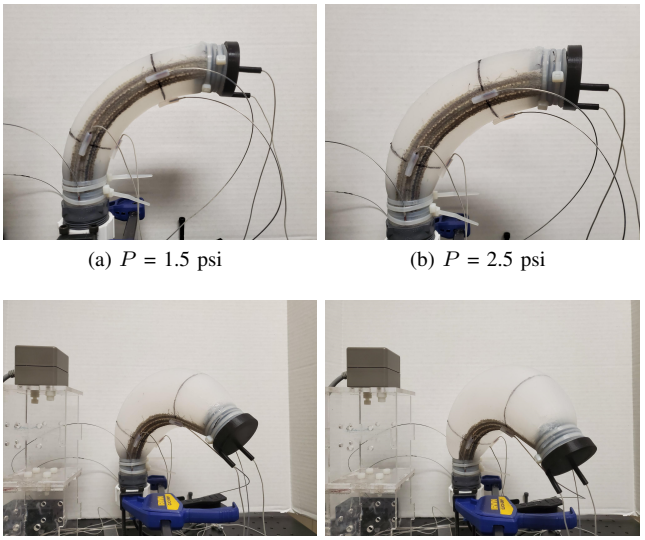

(a) P = 1.5 psi (b) P = 2.5 psi

(c) P = 3 psi (d) P = 3.5 psi

Fig. 2. 4 subsystems represent the whole continuous system

Assumption 1: The generalized contact forces in (5) satisfy the following conditions: $\mathbf{F}_{cj}$ has a derivative and both are upper bounded as $\|\mathbf{F}_{cj}\| \leq L_j$, $\|\dot{\mathbf{F}}_{cj}\| \leq L_j$

In order to estimate the system states and the generalized contact forces, the following Lemma is re-stated to summarize the result of finite-time stability of the dynamical system in the study of Levant and Livne [12]

Lemma 1: Consider the following system:

$$\begin{aligned}
\dot{\varepsilon}_0 &= -\lambda_0|\varepsilon_0|^{n/n+1}sign(\varepsilon_0) - \eta_0\varepsilon_0 + \varepsilon_1, \\
\dot{\varepsilon}_1 &= -\lambda_1|\varepsilon_1 - \dot{\varepsilon}_0|^{(n-1)/n}sign(\varepsilon_1 - \dot{\varepsilon}_0) - \eta_1(\varepsilon_1 - \dot{\varepsilon}_0) \\
&\quad + \varepsilon_2, \\
&\cdots \\
\dot{\varepsilon}_{n-1} &= -\lambda_{n-1}|\varepsilon_{n-1} - \dot{\varepsilon}_{n-2}|^{1/2}sign(\varepsilon_{n-1} - \dot{\varepsilon}_{n-2}) \\
&\quad - \eta_{n-1}(\varepsilon_{n-1} - \dot{\varepsilon}_{n-2}) + \varepsilon_n, \\
\dot{\varepsilon}_n &= -\lambda_n sign(\varepsilon_n - \dot{\varepsilon}_{n-1}) - \eta_n(\varepsilon_n - \dot{\varepsilon}_{n-1}) - \frac{1}{L_0}f(t)
\end{aligned} \tag{6}$$

where n is the relative degree, $\varepsilon_0, ..., \varepsilon_n$ are the state variables, $\lambda_0, ..., \lambda_n$ and $\eta_0, ..., \eta_n$ are appropriate positive scalar constants and the perturbation $f(t)$ satisfies the condition $|f(t)| \leq L_0$ with L_0 a proper positive constant. Then the system converges to the origin in finite time.

Given position data from the marker set, we built a group of observers based on the third order sliding mode approach [12] which has fast convergence and high robustness. The number of observers is the same as the number of subsystems

in (4). The observer for subsystem j is of the form:

$$\begin{aligned}
\dot{\hat{\mathbf{x}}}_{1j} &= \mathbf{M}_j^{-1}\hat{\mathbf{x}}_{2j} - k_{1j}L_j^{1/3}\|\hat{\mathbf{x}}_{1j} - \mathbf{x}_{1j}\|^{2/3}sign(\hat{\mathbf{x}}_{1j} - \mathbf{x}_{1j}) \\
&\quad - k_{2j}(\hat{\mathbf{x}}_{1j} - \mathbf{x}_{1j}) \\
\dot{\hat{\mathbf{x}}}_{2j} &= -k_{3j}L_j^{1/2}\|\mathbf{M}_j^{-1}\hat{\mathbf{x}}_{2j} - \dot{\hat{\mathbf{x}}}_{1j}\|^{1/2}sign(\mathbf{M}_j^{-1}\hat{\mathbf{x}}_{2j} - \dot{\hat{\mathbf{x}}}_{1j}) \\
&\quad - k_{4j}(\mathbf{M}_j^{-1}\hat{\mathbf{x}}_{2j} - \dot{\hat{\mathbf{x}}}_{1j}) + \left(\frac{\partial \mathcal{L}}{\partial \mathbf{q}}\right)_j + \mathbf{Q}_j + \hat{\mathbf{F}}_{cj} \\
\dot{\hat{\mathbf{F}}}_{cj} &= -k_{5j}L_j sign(\mathbf{M}_j^{-1}\hat{\mathbf{x}}_{2j} - \dot{\hat{\mathbf{x}}}_{1j}) \\
&\quad - k_{6j}L_j(\mathbf{M}_j^{-1}\hat{\mathbf{x}}_{2j} - \dot{\hat{\mathbf{x}}}_{1j})
\end{aligned} \tag{7}$$

where $\hat{\mathbf{x}}_{1j}$, $\hat{\mathbf{x}}_{2j}$ are vectors of estimated states, k_{1j} to k_{6j} are the observer gains to be designed and $\hat{\mathbf{F}}_{cj}$ is the vector of estimated generalized contact forces. Note that $\mathbf{x}_{1j}$ can be obtained from the multiplication of the inverse of C_1 and $\mathbf{y}$. Since we have more outputs than the number of states, we can form a non-singular square C_1 so that it is invertible.

Theorem 1: For system (4), if the observer set is designed as in (7) and the observer gains are selected properly, then the estimated states and contact forces will converge to the true values in finite time.

Proof: If the estimation error variables are defined as:

$$\begin{aligned}
\epsilon_{1j} &= \frac{\hat{\mathbf{x}}_{1j} - \mathbf{x}_{1j}}{L_j} \\
\epsilon_{2j} &= \frac{M_j^{-1}(\hat{\mathbf{x}}_{2j} - \mathbf{x}_2)}{L_j} \\
&= \frac{M_j^{-1}\hat{\mathbf{x}}_{2j} - \dot{\hat{\mathbf{x}}}_{1j}}{L_j} \\
&= \frac{M_j^{-1}(\hat{\mathbf{x}}_{2j} - M\dot{\hat{\mathbf{x}}}_{1j})}{L_j} \\
\epsilon_{3j} &= \frac{\hat{F}_{cj} - F_{cj}}{L_j}
\end{aligned} \tag{8}$$

the dynamics of the estimation errors are then obtained as:

$$\begin{aligned}
\dot{\epsilon}_{1j} &= \frac{1}{L_j}(-k_{1j}L_j^{1/3}\|L_j\epsilon_{1j}\|^{2/3}sign(\epsilon_{1j}) - k_{2j}(L_j\epsilon_{1j}) \\
&\quad + M_j^{-1}\hat{\mathbf{x}}_{2j} - M_j^{-1}\mathbf{x}_2) \\
&= -k_{1j}\|\epsilon_{1j}\|^{2/3}sign(\epsilon_{1j}) - k_{2j}(\epsilon_{1j}) + \epsilon_{2j}, \\
\dot{\epsilon}_{2j} &= \frac{1}{L_j}(-k_{3j}L_j^{1/2}\|L_j\epsilon_{2j}\|^{1/2}sign(\epsilon_{2j}) - k_{4j}(L_j\epsilon_{2j}) \\
&\quad + \hat{F}_{cj} - F_{cj}), \\
&= -k_{3j}\|\epsilon_{2j}\|^{1/2}sign(\epsilon_{2j}) - k_{4j}(\epsilon_{2j}) + \epsilon_{3j} \\
\dot{\epsilon}_{3j} &= -k_{5j}sign(\epsilon_{2j}) - k_{6j}\epsilon_{2j} - \frac{1}{L_j}\dot{F}_{cj}
\end{aligned} \tag{9}$$

If the conditions in the Assumption 1 are satisfied, it follows from Lemma 1 that system (9) is finite-time stable, which implies that the estimates converge to true variables in finite time. The detail of how to choose the observer gains can be found in [12]. ■

IV. Simulation and Experimental Results

In this section, we examine the performance of the proposed observer on a four-disc model using some simulated conditions and using data gathered from the physical robot shown in Fig. 1a. The soft robot is discretized into 4 discs and 3 threads. The thread lengths are chosen as $\ell_1 = 7$ cm, $\ell_2 = 9$ cm and $\ell_3 = 7$ cm so that the discs will pass through the marker locations. Note that the robot can be modeled at higher accuracy with higher number of discs but at the cost of higher computational load. For the dimension of the current robot, this 4 disc model can sufficiently describe its behavior. A higher number of discs results in longer expressions without much improvement in model accuracy. To apply the formalism in section III, we choose 4 operating points at 4 increasing pressures including [1.5, 2.5, 3, 3.5] psi (see Fig. 2) and evaluate the matrices $\mathbf{M}$, $\partial\mathcal{L}/\partial\mathbf{q}$ and $\mathbf{Q}$ at these four points to create 4 corresponding subsystems of the form of (3) that represent the entire working range of the soft robot in the form of a switched LPV system (4). During the operating time of the robot, when a new subsystem is switched on due to the changing pressure, the new corresponding observer (7) is switched on as well.

We carry out the simulations for three example cases: 1) no acceleration and no contact for the whole continuous system to estimate the angles q_i, 2) constant acceleration and no contact for the whole continuous system to estimate the rate of change of each q_i, and 3) no acceleration and with contact for the third subsystem to estimate the generalized contact forces. We also conduct an experiment where we inflate the soft robot and collect the real-world marker data to feed into the observer to estimate the states and the corresponding robot poses.

In case study 1) we examine the ability of the observer to estimate the angular positions when changing the input pressure from 1.5 psi to 3.5 psi. The robot is simulated as an LPV system containing 4 subsystems as described at the beginning of this section. The simulation occurs over 4 seconds and is shown in Fig. 3. From the initial time, after each second, the system switches to a new subsystem with different constituent matrices calculated numerically. Each subsystem is illustrated by a different shading from the bright to the darker, each corresponding to higher pressure. There will be, in total, 15 generalized coordinates to track but due to space consideration, only the estimates of a few representative variables are shown. We can see that from their initial values at 0.5 rad, the estimated variables can quickly converge to the true states, in every subsystem.

In case study 2) we assume that the soft robot is undergoing a motion with a constant angular acceleration at 4 mentioned operating points to check the estimation of the angular velocities. Since $\mathbf{q} = \mathbf{M}^{-1}\mathbf{p}$, we can only plot the $\mathbf{p}_i$ and $\mathbf{p}_{i,est}$ in the legends of this figure, instead of the derivatives of the elements of $\mathbf{q}$. Similar to case 1), the simulation runs in 4 seconds and is shown in Fig. 4. It can be observed that the estimates of the angular velocities can quickly converge to true values from their initial values at

5 rad/s, and without steady state errors. There are definitely some biases when switching between the subsystems but the steady observations will be obtained within a short time after entering a new subsystem. Note that the convergence can be smoother at switching points if we linearize the robot by a higher number of subsystems but the LPV system will be more complex. For the current pressurizing range, 4 subsystems are sufficient to evaluate the method with a manageable level of complexity of the LPV system. In this case, the biases happen in a short time with low magnitudes so their effects are not considerable.

In case study 3) we assume the soft robot is in static pose at 3 psi. Hence the simulation is performed for the third subsystem to examine the observer in estimating the generalized contact forces at this operating point. The simulation is run for 6 seconds and is shown in Fig. 5. In this simulation, a contact is applied at $t = 2$ seconds and then removed after 2 more seconds. Each generalized contact force is assumed to have a random value in the range [0; -1] Nm[1]. Our goal is to estimate those generalized contact forces well within the contact time. While the proposed observer can estimate greater forces, the contact forces within 1 Nm in magnitude are introduced and considered as the representative cases to track. As illustrated in the figure, we can see that the designed observer can estimate the assumed generalized contact forces (torques) well during the two-second contact time. The estimates return to zero when the contact is removed. When the contact forces changes their states, there are some overshoots which result from natural response of the observer with the current gains but they happen in very short times and their magnitudes are less than 10% of the changes so they will not have considerable effects on the system model.

Since the disc-thread model represents a discretization of a continuum soft robot, there is no ground truth value against which to compare the state estimates. However, we can compute what the marker locations should be based on the state estimates and compare them to the measured marker location. We inflate and deflate the robot with the input pressure history shown in Fig. 6a. The robot bends down and twists (as can be seen in Fig. 2) when inflated, and returns to the original pose when deflated. The poses of the robot are recorded by the Polhemus electromagnetic motion tracking system. Seven markers are attached on the body of the robot as shown in Fig. 1a to measure the coordinates of each disc.

[1]In fact the generalized contact forces are torques because they are the forces acting on the robot generalized coordinates with lever arms.

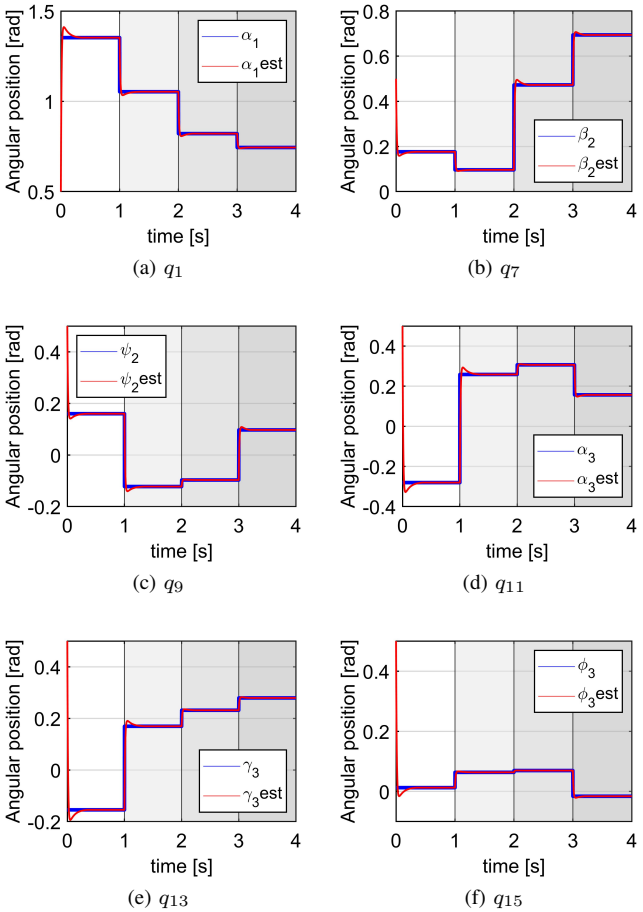

(a) q_1 (b) q_7 (c) q_9 (d) q_{11} (e) q_{13} (f) q_{15}

Fig. 3. (case 1) Estimation of angles q_i

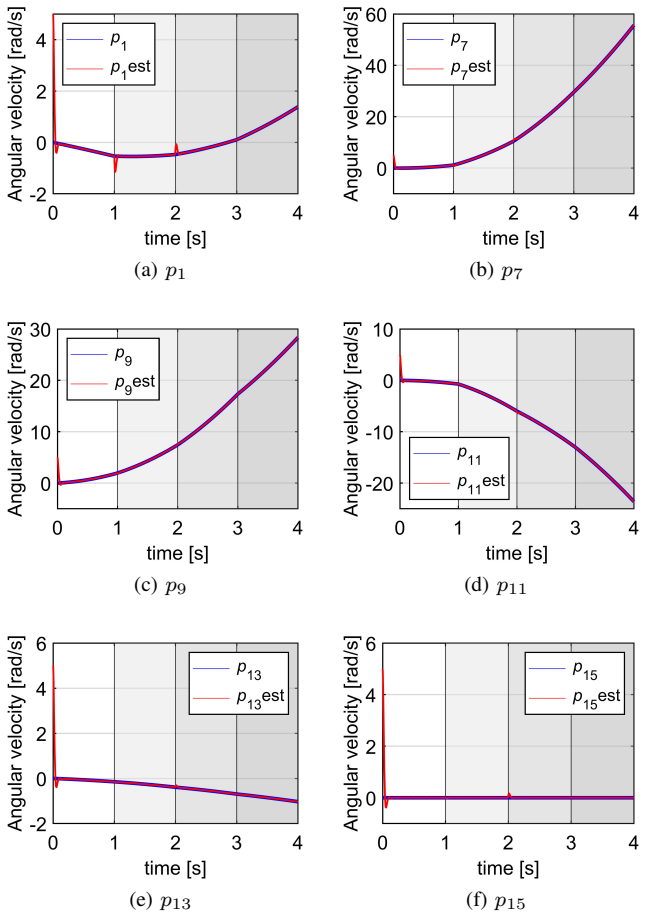

(a) p_1 (b) p_7 (c) p_9 (d) p_{11} (e) p_{13} (f) p_{15}

Fig. 4. (case 2) Estimation of rate of change of $\mathbf{q}_i$. Each p_j is an element of $\mathbf{p}$

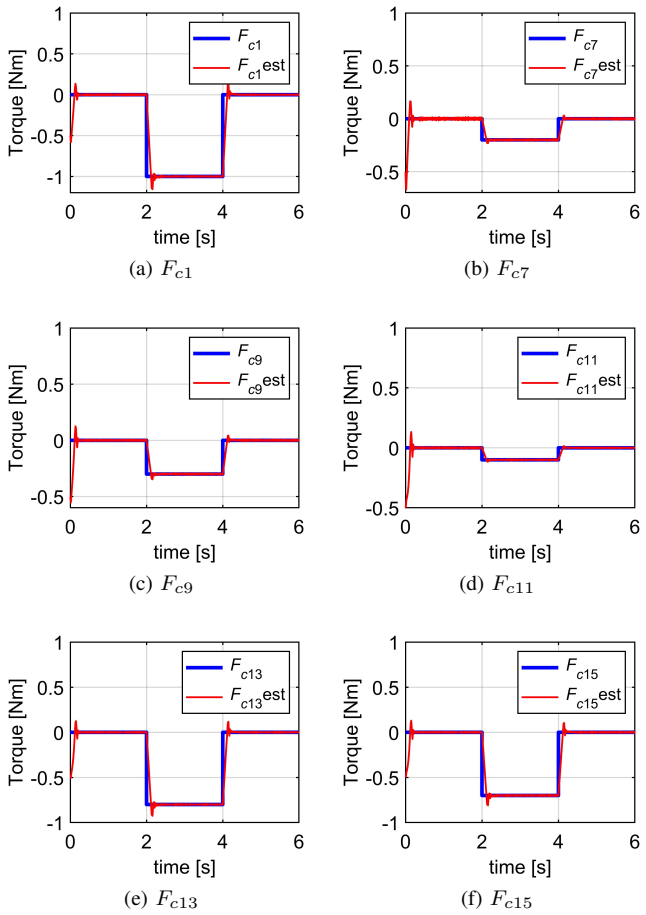

(a) F_{c1} (b) F_{c7}

(c) F_{c9} (d) F_{c11}

(e) F_{c13} (f) F_{c15}

Fig. 5. (case 3) Estimation of generalized contact forces. Each F_{cj} is an element of $\mathbf{F}_c$

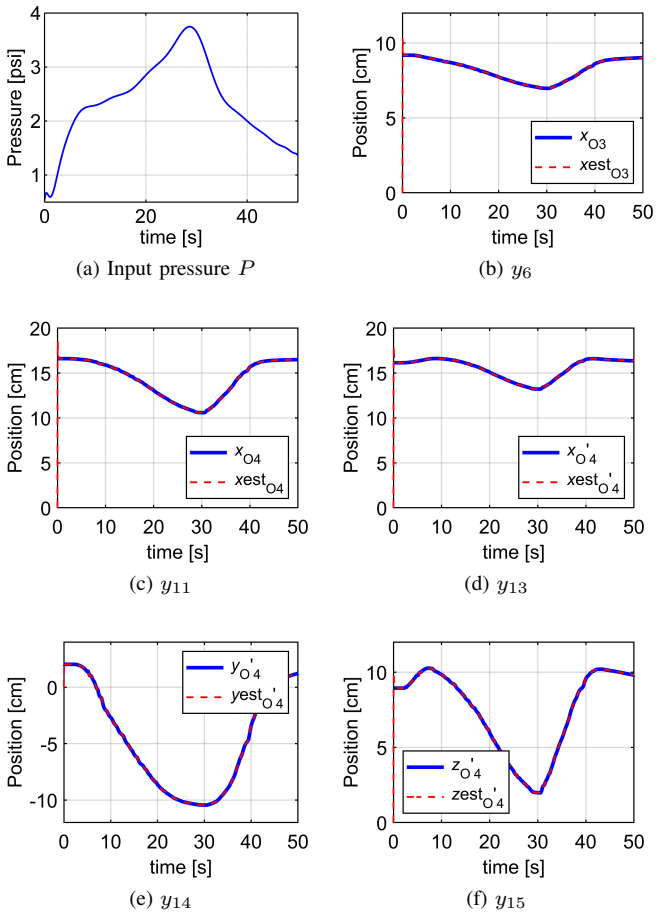

(a) Input pressure P (b) y_6

(c) y_{11} (d) y_{13}

(e) y_{14} (f) y_{15}

Fig. 6. Estimation of measured marker coordinates

We then feed data measured from the tracking system into the observer. The estimated outputs $\hat{\mathbf{y}} = C_1\hat{\mathbf{x}}_1$ are compared to the real outputs measured from the markers. The results are illustrated in Fig. 6. We can see that the postures of the soft robot represented by marker coordinates are well estimated and the estimates quickly converge to the marker coordinates from their initial values at zero. This indicates that the estimated states of the real robot obtained by the observer are plausible and can be used for model-based control design. Note that the experiment took 50 seconds in order that the pressure was manually controlled smoothly as shown in Fig.6a. While the time span in the simulation can be of any duration, it was set as only 4 seconds so that readers can recognize the rise time of the estimates easily. In general, the performance of the observer in simulation and in response to experimental data shows that it works well for this class for the disc-thread model of fabric-reinforced soft robots.

V. Conclusion

In this paper, we propose an observer to estimate the generalized states and contact forces for a fabric-reinforced inflatable robot as represented by a new disc-thread model approach. Simulations and experiments are performed to examine the behavior of the observer. The results show that the observer works well in simulation by converging to static poses and motion due to changing pressure as well as estimating an assumed contact case. The performance of the observer is also confirmed via an experiment where it can estimate the pose of the soft robot using the data from the position marker set. Interestingly, by applying this modeling approach and observer design, we may exploit well-developed model-based linear control theory for a class of inflatable soft robots. Although the control schemes for soft robots are definitely different from those for traditional robots, the ability to apply traditional control algorithms can provide stability guarantees and save a lot of works in controller design. We plan to design a model-based controller to perform position tracking with this soft robot in our future research. In addition, future work will treat the case when contact occurs suddenly by collision with an object in the environment. Pose estimation under a real-world contact will also be considered. It is likely that machine learning methods will be used in tandem with this observer design to more reliably estimate the contact force when the environment is poorly known.

REFERENCES

[1] F. lida and C. Laschi, "Optimization-based inverse model of soft robots with contact handling," *Procedia Computer Science*, vol. 7, pp. 99–102, December 2011.

[2] T. G. Thuruthel, Y. Ansari, E. Falotico, and C. Laschi, "Control strategies for soft robotic manipulators: A survey," *Soft robotics*, vol. 5, pp. 149–163, April 2018.

[3] E. Coevoet, A. Escande, and C. Duriez, "Optimization-based inverse model of soft robots with contact handling," *IEEE Robotics and automation letters*, vol. 2, pp. 1413–1419, July 2017.

[4] C. D. Santina, R. L. Truby, and D. Rus, "Data–driven disturbance observers for estimating external forces on soft robots," *IEEE Robotics and automation letters*, vol. 5, pp. 5717–5724, October 2020.

[5] Z. Zhang, J. Dequidt, A. Kruszewski, F. Largilliere, and C. Duriez, "Kinematic modeling and observer based control of soft robot using real-time finite element method," in *2016 IEEE/RSJ International Conference on Intelligent Robots and Systems*, Daejeon, Korea, October 2016, pp. 5509–5514.

[6] M. T. Gillespie, C. M. Best, and M. D. Killpack, "Simultaneous position and stiffness control for an inflatable soft robot," in *2016 IEEE International Conference on Robotics and Automation (ICRA)*, Stockholm, Sweden, May 2016, pp. 1095–1101.

[7] A. Ataka, P. Qi, A. ShivaI, A. Shafti, H. Wurdemann, H. Liu, and K. Althoefer, "Real-time pose estimation and obstacle avoidance for multi-segment continuum manipulator in dynamic environments," in *2016 IEEE/RSJ International Conference on Intelligent Robots and Systems (IROS)*, Daejeon, Korea, October 2016, pp. 2827–2832.

[8] W. S. Rone and P. Ben-Tzvi, "Multi-segment continuum robot shape estimation using passive cable displacement," in *ROSE 2013 - IEEE International Symposium on Robotic and Sensors Environments*, Washington, USA, October 2013, pp. 37–42.

[9] R. A. Srivatsan, M. Travers, and H. Choset, "Using Lie algebra for shape estimation of medical snake robots," in *2014 IEEE/RSJ International Conference on Intelligent Robots and Systems (IROS 2014)*, Chicago, USA, Septemberr 2014, pp. 3483–3488.

[10] J. A. Schultz, H. Sanders, P. D. H. Bui, M. W. Keller, and M. Killpack, "Representing fabric-reinforced inflatable robots by discs and threads," in *International Mechatronics Conference and Workshops*, Oklahoma City, USA, October 2020, p. to appear.

[11] J. G. Williamson, C. Schell, M. Keller, and J. Schultz, "Extending the reach of single-chamber inflatable soft robots using Magnetorheological Fluids," in *IEEE International Conference on Soft Robotics*, New Haven, Connecticut, April 2021, p. to appear.

[12] A. Levant and M. Livne, "Globally convergent differentiators with variable gains," *International Journal of Control*, vol. 91, pp. 1994–2008, March 2018.